Computational Geosciences (2021) 25:655–669
https://doi.org/10.1007/s10596-020-09986-x

ORIGINAL PAPER

# Numerical modeling of a memory-based diffusivity equation and determination of its fractional order value

Tareq Uz Zaman[1] · Scott MacLachlan[2] · M. Enamul Hossain[3]

Received: 29 May 2019 / Accepted: 15 June 2020 / Published online: 14 July 2020


**Abstract**

Conventional diffusion equations for fluid flow through porous media do not consider the effects of the history of rock, fluid, and flow. This limitation can be overcome by the incorporation of "memory" in the model, using fractional-order derivatives. Inclusion of fractional-order derivatives in the diffusion equation, however, adds complexity to both the equation and its numerical approximation. Of particular importance is the choice of temporal mesh, which can dramatically affect the convergence of the scheme. In this article, we consider a memory-based radial diffusivity equation, discretized on either uniform or graded meshes. Numerical solutions obtained from these models are compared against analytical solutions, and it is found that the simulation using properly chosen graded meshes gives substantially smaller errors compared to that using uniform meshes. Experimental data from one-dimensional flow through a porous layer with constant pressure gradient are collected from the literature and used to fit the fractional order in the diffusivity equation considered here. A reasonable value of the fractional order is found to be 0.05; this is further validated by performing numerical simulations to match these experiments, demonstrating substantial improvement over the classical Darcy's model.

**Keywords** Reservoir simulation · Memory · Fractional derivatives · Graded meshes

## 1 Introduction

Reservoir modeling is crucial for the development, planning, and production management of oil and gas fields. It aids in the decision-making process throughout all stages of field life. Numerous mathematical models have been developed for different types of reservoirs and fluids over more than the past 50 years, modeling various flow regimes and properties. In recent years, researchers have started to investigate the effects of the history of the rock, fluid, and flow, also known as memory, on flow through porous media. The recent literature on the mathematical modeling of rock/fluid interactions in porous media shows that many researchers are developing models incorporating memory effects [1–6].

Properties of both the rock and fluid change with time while fluid flows through porous media. Pores of the medium might be enlarged, due to chemical reactions between the medium and the fluid, or can be diminished or even closed, due to deposition of solid particles carried by the fluid or by the precipitation of minerals from the fluid. Hence, the reservoir rock, fluid, and flow properties (e.g., porosity, permeability, surface tension, viscosity, fluid saturation, wettability, reservoir thickness, pressure, and temperature) are functions of time. Such variation of rock-fluid properties with time in a reservoir can be defined as the memory and is typically included in mathematical models by the use of fractional derivatives. These fractional temporal derivatives can be used to account for the continuous alteration of the rock-fluid rheology. Caputo and Plastino [7] used fractional temporal derivatives to model possible changes in the physical properties of the media due to variations in its temperature and physical or

✉ Tareq Uz Zaman
tzaman@mun.ca

Scott MacLachlan
smaclachlan@mun.ca

M. Enamul Hossain
dr.mehossain@gmail.com

[1] Oil and Gas Engineering Program, Memorial University of Newfoundland, St. John's, Canada

[2] Department of Mathematics and Statistics, Memorial University of Newfoundland, St. John's, Canada

[3] Department of Petroleum and Energy Engineering, American University in Cairo, Cairo, Egypt

chemical interactions with the fluid. Iaffaldano et al. [8] used fractional temporal derivatives to model compaction effects. In [2] and [9], the changes of the physical properties of the fluid and porous media with time were modeled using fractional temporal derivatives.

Several heuristic definitions of memory are found in the literature. Zhang [6] defined memory as a function of time and space, where forward time events depend on previous time events. Christensen [3] defined memory to be when the history of the deformation and fractures of a solid under stress is used to determine the propagation of a fracture within a solid. Zavala-Sanchez et al. [5] showed that a system can remember its initial state, defining memory effects for the effective transport coefficients. Hossain et al. [4] defined memory as the effect of past events on the present and future course of developments. In this direction, Hossain et al. [10] proposed the following diffusivity equation:

$$\frac{\partial}{\partial x}\left[\frac{\rho k}{\mu}\tau^{\alpha}\frac{\partial^{\alpha}}{\partial t^{\alpha}}\left(\frac{\partial p}{\partial x}\right)\right]=\rho\phi c_t\frac{\partial p}{\partial t}, \tag{1}$$

where $p$ is the fluid pressure, $\rho$ the fluid density, $\phi$ the porosity of the medium, $k$ the permeability of the medium, $\mu$ the dynamic viscosity of the fluid, $c_t$ the total compressibility of the system, $\alpha$ the fractional order of differentiation, and $\tau$ the relaxation time. Instead of treating the fractional-order derivative by its definition and discretizing Eq. 1 directly, Hossain et al. [10] considered the term as a parameter, solving the equation numerically as an integer-order partial differential equation. Hence, their numerical solution is not accurate in the mathematical sense. A contrasting model, used in [1] considers only a single (fractional) time derivative, as

$$\frac{\partial}{\partial x}\left[\frac{\rho k}{\mu}\tau^{\alpha}\frac{\partial p}{\partial x}\right]=\rho\phi c_t\frac{\partial^{1-\alpha}p}{\partial t^{1-\alpha}}. \tag{2}$$

We note those two formulations are equivalent only in the case of physical coefficients that have no dependence on time, either directly or through constitutive relations that depend on $p(x,t)$, which is not relevant to most reservoir simulation settings. In what follows, we explicitly consider the diffusivity equation in the form of Eq. 1 to allow spatially varying and nonlinear coefficients.

The fractional-order derivative should be properly included in the diffusion equation in order to incorporate memory in a numerical model. However, inclusion of the fractional-order derivative makes the diffusion equation difficult to solve both analytically and numerically, due to the non-local behavior of the fractional-order derivative. Numerous studies on numerical approaches to fractional diffusion equations are found in the literature applying standard discretization techniques to this case. Many authors have applied finite-difference methods [11–30], while others have applied finite-element methods [31, 32]. Some authors have used the Riemann-Liouville definition of fractional-order derivatives [11–15, 18, 21, 22, 26, 28], while others have used the Caputo definition [16, 17, 20, 23–25, 29]. Liu et al. [19] used the Riemann-Liouville definition for a spatial fractional-order derivative and the Caputo definition for a temporal fractional-order derivative.

Among the finite-difference papers, Chen et al. [12] presented an implicit approximation scheme for solving a fractional partial differential equation describing sub-diffusion. Cui [15] used the Grunwald-Letnikov discretization of the Riemann-Liouville derivative to obtain a fully discrete implicit scheme for solving a one-dimensional fractional diffusion equation. Liu et al. [19] investigated a fractional order implicit finite-difference approximation for the space-time-fractional diffusion equation. Liu et al. [20] developed an implicit meshless approach based on the radial basis function (RBF) methodology to solve time-fractional diffusion equations. Zhuang et al. [29] proposed an implicit difference approximation to solve time-fractional diffusion equations, based on the L1 approximation for Caputo time-fractional derivatives. An implicit finite-difference scheme using the L1 formula was constructed by Sun et al. [25] for solving a diffusion-wave system. On the other hand, Murillo et al. [24] solved fractional diffusion and fractional diffusion-wave equations applying an explicit difference method. Yuste et al. [28] obtained an explicit forward-time centered-space method, combining the standard forward-time centered-space method with the Grunwald-Letnikov discretization of the Riemann-Liouville derivative for solving the fractional diffusion equation. Lynch et al. [21] developed an explicit and a semi-implicit numerical scheme to solve an anomalous diffusion problem. Chen et al. [33] solved fractional reaction-subdiffusion equations, applying both implicit and explicit finite-difference methods.

Chen et al. [14] proposed a numerical scheme with first-order temporal accuracy and fourth-order spatial accuracy for a variable-order anomalous subdiffusion equation. Gao et al. [17] applied the L1 discretization for the time-fractional part and a fourth-order accurate compact approximation for the second-order space derivative to solve the fractional subdiffusion equations. Tadjeran et al. [26] combined the classical Crank-Nicholson method with spatial extrapolation to obtain temporally and spatially second-order accurate numerical estimates for fractional-order diffusion equations. These schemes achieve these orders only for smooth-enough solutions.

It is important to emphasize that all of these articles use uniform meshes in space and time and assume high regularity of the continuum solution. However, Stynes et al. [34] show that "typical" solutions of equations such as Eq. 1 do not possess enough regularity for these bounds to be

useful. In particular, solutions of Eq. 1 are expected to have much steeper initial decay than those of the classical heat equation, but with much slower long-term decay. Thus, they defined and used graded meshes in time for the class of time-dependent problems in Eq. 2 with a single fractional temporal derivative of order $(1-\alpha) \in (0, 1)$. The use of the graded mesh greatly affects the order of convergence of the difference scheme for "typical" solutions of such an equation. Though this work provides a very good theoretical prescription for the time-fractional heat equation, it is not one that can be immediately applied to porous media, particularly in the form of Eq. 1 with coefficients that may vary in both space and time and depend on the solution, $p(x, t)$. Furthermore, there is a big difference between Eq. 1 and Eq. 2, where only one time derivative of order $(1-\alpha)$ appears on the right-hand side due to multiplication by the other coefficients in Eq. 1. The Stynes et al.'s paper [34] motivated us to use graded meshes in time to solve Eq. 1 numerically, bringing the theoretically motivated technique from [34] into realistic (but one-dimensional) models of porous media flow.

In this paper, the model of Hossain et al. [10] is solved numerically using the Riemann-Liouville definition of the fractional-order derivative for both uniform and graded meshes. For graded meshes, the uniform mesh L1 algorithm [35] using the Riemann-Liouville definition for fractional-order derivatives is adapted to discretize the diffusivity equation. The numerical models developed utilizing uniform and graded meshes are studied and compared. The relationship between the optimal number of steps in unit time and number of grid-points in unit length is found for different values of $\alpha$. The value of the fractional order, $\alpha$, in Hossain et al.'s [10] model has been calculated for experimental data collected from literature.

This paper is arranged as follows. In Section 2, Eq. 1 is discretized for both uniform and graded temporal meshes. The computational algorithm is presented, and errors found from uniform and graded meshes are compared. In Section 3, we determine the value of the fractional-order, $\alpha$, for Eq. 1 from experimental data. The optimal number of time steps for graded meshes is determined in Section 4 and used to perform simulations to compare against these experiments.

## 2 Discretization schemes and validation

The simplest model used to describe flow in porous media is Darcy's law, which relates the pressure gradient to the volumetric flux through the viscosity of the fluid and the permeability of the medium. Darcy's law models only the viscous pressure drop and not the inertial pressure drop; as a result, Darcy's law is only applicable to the laminar flow regime and cannot model the nonlinear flow regime, where pressure drops due to inertial effects are no longer negligible. Darcy's law also does not consider the effects of memory. Therefore, the application of Darcy's law is limited to laminar, isothermal, purely viscous, incompressible Newtonian flow [36]. While significant modeling can be done using Darcy's law, more detailed models are needed for non-conventional flow regimes.

### 2.1 Memory concept in flow modeling

In conventional reservoir models, the effects of the history of the rock, fluid, and flow properties on flow phenomena are not considered. However, in recent literature, some mathematical models are found that are based on the fact that fluid flow phenomena through porous media depend on their past [2, 8, 10]. When a complex fluid flows through a porous medium, there is a change in both the rock and fluid properties due to chemical reactions, mineral precipitation, and other processes and, therefore, permeability and viscosity change over time. This phenomenon, that rock and fluid properties change over time, is represented by the term "memory". To quantify the effect of history, memory is incorporated into the mathematical model. Two types of memory, time memory and space memory, are found in literature. Space memory considers the previous space that the fluids have passed through [37], while time memory fixes a location in space and considers the time history of the flow at that point [1, 2].

Memory is incorporated in mathematical models of reservoirs using fractional-order derivatives in the model, as the definition of these derivatives provides a natural way to include history. The history of the pressure, pressure gradients, or any other parameters can be taken into consideration using fractional-order derivatives of that parameter.

Once fractional-order derivatives come into the model to incorporate memory, the equations become complicated and are difficult to solve either analytically or numerically. Unlike integer-order derivatives, fractional-order derivatives do not have a single definition. Different definitions produce different equations and substantially different solutions for the same model. Selecting a suitable definition for the fractional-order derivative for specific initial and boundary conditions, and developing new schemes and algorithms to handle the fractional-order diffusivity equation are great challenges.

In Eq. 1, the model contains a first derivative in time and the fractional derivative mixed within the spatial derivatives. For the constant-coefficient case, the solutions can be derived via separation of variables and the Laplace transform. If the Caputo derivative is used there, the only solutions found are constant in time. However, use of the

Riemann-Liouville definition gives the solutions in terms of Mittag-Leffler functions. Due to this fact, the Riemann-Liouville definition has been used here. See Appendix A for more details.

## 2.2 Discretization using uniform meshes

The mathematical model (Eq. 1) is discretized using a finite-difference method. For some positive value $X$ and integer $N_x$, the grid size in space is defined by $\Delta x = X/N_x$. The grid points in the space interval $[0, X]$ are given by $x_i = i\,\Delta x$, $i = 0, 1, 2, ..., N_x$. In the case of a uniform mesh in time, for some positive value $T$ and integer $N_t$, the grid size is defined by $\Delta t = T/N_t$. The grid points in the time interval $[0, T]$ are labeled $t_n = n\Delta t$, $n = 0, 1, 2, ..., N_t$. The values of a function $p(x, t)$ at the grid points are denoted by $p_i^n = p(x_i, t_n)$.

Denoting $C_1(x,t) = \frac{\rho k}{\mu}\tau^\alpha$ and $C_2(x,t) = \rho\phi c_t$ in Eq. 1 gives

$$\frac{\partial}{\partial x}\left[C_1(x,t)\frac{\partial^\alpha}{\partial t^\alpha}\left(\frac{\partial p}{\partial x}\right)\right]_i^n = C_2(x_i,t_n)\frac{\partial p_i^n}{\partial t}. \tag{3}$$

Discretizing this using implicit Euler in time and centered differences in space, writing $F^n_{(i\pm\frac{1}{2})} = \left[C_1\frac{\partial^\alpha}{\partial t^\alpha}(\frac{\partial p}{\partial x})\right]^n_{(i\pm\frac{1}{2})}$ gives

$$\frac{1}{\Delta x}(F^n_{i+\frac{1}{2}} - F^n_{i-\frac{1}{2}}) = C_2(x_i,t_n)\frac{p_i^n - p_i^{n-1}}{\Delta t}. \tag{4}$$

To represent the fractional derivative, we use the L1 algorithm [35], writing

$$\frac{\partial^\alpha u(x_{i\pm\frac{1}{2}},t_n)}{\partial t^\alpha} = \frac{t_n^{-\alpha}n^\alpha}{\Gamma(2-\alpha)}\left[\frac{1-\alpha}{n^\alpha}u(x_{i\pm\frac{1}{2}},0) + \sum_{j=0}^{n-1}\left(u(x_{i\pm\frac{1}{2}},t_n - t_j) - u\left(x_{i\pm\frac{1}{2}},t_n - t_{j+1}\right)\right)\times\left((j+1)^{1-\alpha} - j^{1-\alpha}\right)\right].$$

Using this and approximating $\frac{\partial p(x_{i+\frac{1}{2}},t_n)}{\partial x} \approx \frac{1}{\Delta x}\left(p\left(x_{i+1},t_n\right) - p\left(x_i,t_n\right)\right)$, $F^n_{i+\frac{1}{2}}$ and $F^n_{i-\frac{1}{2}}$ can be written as

$$F^n_{i+\frac{1}{2}} = \frac{1}{\Delta x}C_1(x_{i+\frac{1}{2}},t_n)\sigma_{\alpha,\Delta t}\left[\frac{1-\alpha}{n^\alpha}(p_{i+1}^0 - p_i^0) + p_{i+1}^n - p_i^n - p_{i+1}^{n-1} + p_i^{n-1} + \sum_{j=1}^{n-1}\omega_j^{(\alpha)}(p_{i+1}^{n-j} - p_i^{n-j} - p_{i+1}^{n-j-1} + p_i^{n-j-1})\right], \tag{5}$$

and

$$F^n_{i-\frac{1}{2}} = \frac{1}{\Delta x}C_1(x_{i-\frac{1}{2}},t_n)\sigma_{\alpha,\Delta t}\left[\frac{1-\alpha}{n^\alpha}(p_i^0 - p_{i-1}^0) + p_i^n - p_{i-1}^n - p_i^{n-1} + p_{i-1}^{n-1} + \sum_{j=1}^{n-1}\omega_j^{(\alpha)}(p_i^{n-j} - p_{i-1}^{n-j} - p_i^{n-j-1} + p_{i-1}^{n-j-1})\right], \tag{6}$$

where

$$\omega_j^{(\alpha)} = (j+1)^{1-\alpha} - j^{1-\alpha} \quad \text{and} \quad \sigma_{\alpha,\Delta t} = \frac{1}{\Delta t^\alpha\Gamma(2-\alpha)}.$$

Substitution of Eqs. 5 and 6 into Eq. 4 gives

$$\begin{aligned} &- C_1(x_{i-\frac{1}{2}},t_n)p_{i-1}^n \\ &+ \left[C_1(x_{i-\frac{1}{2}},t_n) + C_1(x_{i+\frac{1}{2}},t_n) + \frac{C_2(x_i,t_n)\Delta x^2}{\sigma_{\alpha,\Delta t}\Delta t}\right]p_i^n \\ &- C_1(x_{i+\frac{1}{2}},t_n)p_{i+1}^n = \frac{C_2(x_i,t_n)\Delta x^2}{\sigma_{\alpha,\Delta t}\Delta t}p_i^{n-1} \\ &\quad + C_1(x_{i+\frac{1}{2}},t_n)G_i^n - C_1(x_{i-\frac{1}{2}},t_n)H_i^n, \end{aligned} \tag{7}$$

where we collect the sums over past time steps into

$$G_i^n = \tfrac{1-\alpha}{n^\alpha}(p_{i+1}^0 - p_i^0) - p_{i+1}^{n-1} + p_i^{n-1} + \sum_{j=1}^{n-1}\omega_j^{(\alpha)}(p_{i+1}^{n-j} - p_i^{n-j} - p_{i+1}^{n-j-1} + p_i^{n-j-1}),$$

and

$$H_i^n = \tfrac{1-\alpha}{n^\alpha}(p_i^0 - p_{i-1}^0) - p_i^{n-1} + p_{i-1}^{n-1} + \sum_{j=1}^{n-1}\omega_j^{(\alpha)}(p_i^{n-j} - p_{i-1}^{n-j} - p_i^{n-j-1} + p_{i-1}^{n-j-1}).$$

## 2.3 L1 algorithm for graded meshes

Motivated by Stynes et al.'s grading of the meshes in time [34], the memory-based diffusion equation (Eq. 1) is discretized on graded meshes. These meshes aim to capture the fast initial decay of typical solutions to fractional diffusion equations by using small time steps for early times and larger time steps as simulation proceeds. For the graded mesh, the local grid size is defined by $\Delta t_n = t_n - t_{n-1}$. The grid points in the time interval $[0, T]$ are labeled $t_n = T(n/N_t)^\omega, n = 0, 1, 2, ..., N_t$ where the constant mesh grading $\omega \geq 1$ is adapted from [34]. In the notation of Eq. 1, $\omega = (1+\alpha)/(1-\alpha)$ matches the choice recommended in [34] for a Caputo derivative of order $1-\alpha$ in Eq. 2.

The L1 algorithm is derived for non-uniform mesh grading using the Riemann-Liouville definition for fractional-order derivatives. From its definition, the Riemann-Liouville fractional derivative for $0 \leq \alpha < 1$ is given by

$$\frac{d^\alpha u}{dt^\alpha} \approx \frac{1}{\Gamma(1-\alpha)} \left[ \frac{u(0)}{t^\alpha} + \sum_{j=0}^{N_t-1} \int_{t_j}^{t_{j+1}} \frac{du(y)}{dy} \frac{dy}{(t-y)^\alpha} \right] \quad (8)$$

The L1 algorithm utilizes the approximation

$$\begin{aligned} \int_{t_j}^{t_{j+1}} \frac{du(y)}{dy} \frac{dy}{(t-y)^\alpha} &\approx \frac{u(t_{j+1})-u(t_j)}{t_{j+1}-t_j} \int_{t_j}^{t_{j+1}} \frac{dy}{(t-y)^\alpha} \\ &\approx \frac{1}{1-\alpha} \frac{u(t_{j+1})-u(t_j)}{t_{j+1}-t_j} \\ &\times \left[ (t-t_j)^{1-\alpha} - (t-t_{j+1})^{1-\alpha} \right]. \end{aligned} \quad (9)$$

Substitution of Eq. 9 into Eq. 8 gives

$$\left[ \frac{d^\alpha u}{dt^\alpha} \right]_{L1} \approx \frac{1}{\Gamma(1-\alpha)} \left[ \frac{u(0)}{t^\alpha} + \sum_{j=0}^{N_t-1} \frac{1}{1-\alpha} \frac{u(t_{j+1})-u(t_j)}{t_{j+1}-t_j} \times \left( (t-t_j)^{1-\alpha} - (t-t_{j+1})^{1-\alpha} \right) \right]. \quad (10)$$

Eq. 10 can be written as

$$\left[ \frac{d^\alpha u}{dt^\alpha} \right]_{L1} \approx \frac{1}{\Gamma(2-\alpha)} \left[ \frac{(1-\alpha)u(0)}{t^\alpha} + \sum_{j=0}^{N_t-1} \frac{u(t_{j+1})-u(t_j)}{t_{j+1}-t_j} \times \left( (t-t_j)^{1-\alpha} - (t-t_{j+1})^{1-\alpha} \right) \right]. \quad (11)$$

Eq. 11 is the L1 algorithm for non-uniform mesh spacing for the Riemann-Liouville definition of the fractional-order derivative. We note that in comparison to the Caputo case considered in Eq. (3.1) of [34], the only difference is the presence of an additional term depending on the initial data; however, Eq. 15 below is significantly different than the discretization arising from using the Caputo derivative of order $(1-\alpha)$ in place of the derivative on the Darcy velocity.

### 2.4 Numerical solution for graded meshes in time

Discretizing Eq. 3 using implicit Euler in time and staggered finite differences in space with $F^n_{(i\pm\frac{1}{2})} = \left[ C_1 \frac{\partial^\alpha}{\partial t^\alpha} (\frac{\partial p}{\partial x}) \right]^n_{(i\pm\frac{1}{2})}$ gives

$$\frac{1}{\Delta x}(F^n_{i+\frac{1}{2}} - F^n_{i-\frac{1}{2}}) = C_2(x_i, t_n) \frac{p_i^n - p_i^{n-1}}{t_n - t_{n-1}}. \quad (12)$$

Using the L1 algorithm derived in Eq. 11, $F^n_{i+\frac{1}{2}}$ and $F^n_{i-\frac{1}{2}}$ can be written as

$$\begin{aligned} F^n_{i+\frac{1}{2}} = \frac{1}{\Delta x \Gamma(2-\alpha)} C_1(x_{i+\frac{1}{2}}, t_n) \Bigg[ &\frac{1-\alpha}{(t_n)^\alpha}(p^0_{i+1} - p^0_i) \\ &+ (t_n - t_{n-1})^{-\alpha}(p^n_{i+1} - p^n_i) - (t_n - t_{n-1})^{-\alpha}(p^{n-1}_{i+1} - p^{n-1}_i) \\ &+ \sum_{j=0}^{n-2} \frac{\left[ (t_n - t_j)^{1-\alpha} - (t_n - t_{j+1})^{1-\alpha} \right]}{(t_{j+1} - t_j)} \\ &\times (p^{j+1}_{i+1} - p^{j+1}_i - p^j_{i+1} + p^j_i) \Bigg], \end{aligned} \quad (13)$$

and

$$\begin{aligned} F^n_{i-\frac{1}{2}} = \frac{1}{\Delta x \Gamma(2-\alpha)} C_1(x_{i-\frac{1}{2}}, t_n) \Bigg[ &\frac{1-\alpha}{(t_n)^\alpha}(p^0_i - p^0_{i-1}) \\ &+ (t_n - t_{n-1})^{-\alpha}(p^n_i - p^n_{i-1}) \\ &- (t_n - t_{n-1})^{-\alpha}(p^{n-1}_i - p^{n-1}_{i-1}) \\ &+ \sum_{j=0}^{n-2} \frac{\left[ (t_n - t_j)^{1-\alpha} - (t_n - t_{j+1})^{1-\alpha} \right]}{(t_{j+1} - t_j)} \\ &\times (p^{j+1}_i - p^{j+1}_{i-1} - p^j_i + p^j_{i-1}) \Bigg]. \end{aligned} \quad (14)$$

Substitution of Eqs. 13 and 14 into Eq. 12 gives

$$\begin{aligned} &- C_1(x_{i-\frac{1}{2}}, t_n) p^n_{i-1} + \Big[ C_1(x_{i-\frac{1}{2}}, t_n) + C_1(x_{i+\frac{1}{2}}, t_n) \\ &+ C_2(x_i, t_n) \Delta x^2 \Gamma(2-\alpha)(t_n - t_{n-1})^{\alpha-1} \Big] p^n_i \\ &- C_1(x_{i+\frac{1}{2}}, t_n) p^n_{i+1} \\ &= C_2(x_i, t_n) \Delta x^2 \Gamma(2-\alpha)(t_n - t_{n-1})^{\alpha-1} p^{n-1}_i \\ &+ C_1(x_{i+\frac{1}{2}}, t_n)(t_n - t_{n-1})^\alpha \widehat{G}^n_i \\ &\quad - C_1(x_{i-\frac{1}{2}}, t_n)(t_n - t_{n-1})^\alpha \widehat{H}^n_i, \end{aligned} \quad (15)$$

where

$$\begin{aligned} \widehat{G}^n_i = &\tfrac{(1-\alpha)}{(t_n)^\alpha}(p^0_{i+1} - p^0_i) - (t_n - t_{n-1})^{-\alpha}(p^{n-1}_{i+1} - p^{n-1}_i) \\ &+ \sum_{j=0}^{n-2} \tfrac{\left[ (t_n - t_j)^{1-\alpha} - (t_n - t_{j+1})^{1-\alpha} \right]}{t_{j+1} - t_j} \\ &\times (p^{j+1}_{i+1} - p^{j+1}_i - p^j_{i+1} + p^j_i), \end{aligned}$$

and

$$\begin{aligned} \widehat{H}^n_i = &-\tfrac{(1-\alpha)}{(t_n)^\alpha}(p^0_i - p^0_{i-1}) - (t_n - t_{n-1})^{-\alpha}(p^{n-1}_i - p^{n-1}_{i-1}) \\ &+ \sum_{j=0}^{n-2} \tfrac{\left[ (t_n - t_j)^{1-\alpha} - (t_n - t_{j+1})^{1-\alpha} \right]}{t_{j+1} - t_j} \\ &\times (p^{j+1}_i - p^{j+1}_{i-1} - p^j_i + p^j_{i-1}). \end{aligned}$$

Figure 1 shows the computational algorithm used herein to solve the numerical models developed for both uniform and graded meshes. Equations 7 and 15 are written for each grid point and, then, the system of equations for each case is solved. Note, however, that the equations can be nonlinear: the pressures depend on the density, permeability, viscosity, porosity, and compressibility which, themselves,

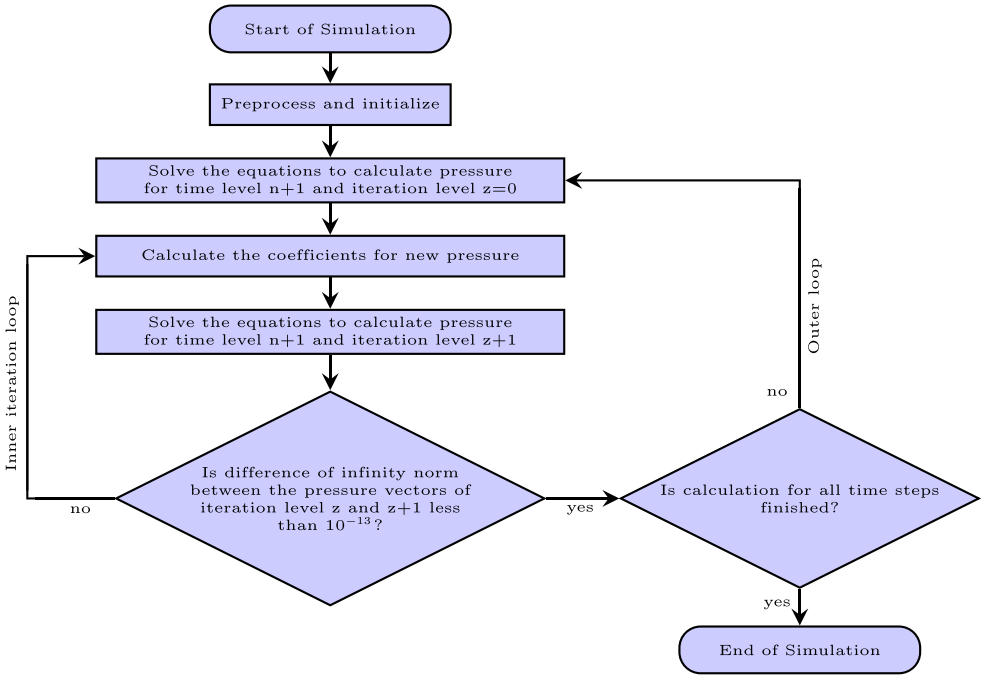


**Fig. 1** Computational algorithm to solve the numerical model

may depend on these pressures. Thus, a simple iterative scheme (fixed point iteration) is used to update the density, permeability, viscosity, porosity, and compressibility. The approach is illustrated qualitatively by

$$A(\rho, k, \mu, \phi, c_t)^{n,z} p^{n,z+1} = RHS^{n,z}.$$

For each time step and each inner iteration, the pressure, density, permeability, viscosity, porosity, and compressibility data are assumed known from the most recent computational value. At the start of a new time step, the most recent value is that from the solution at the previous time step, while during a given time step it is that from the last iteration. The coefficients are updated using the new values of pressure as the pressures are updated and this process is continued. The iteration process terminates when the convergence criterion is satisfied. Two MATLAB programs have been written based on Eqs. 7 and 15 to numerically solve Eq. 1 for uniform and graded meshes in time, respectively. We note that a more sophisticated linearization scheme (e.g., based on Newton's method) is certainly possible here, but focus on the simplest linearization to emphasize the role of the temporal mesh, and not the details of the time-stepping procedure. Similarly, greater computational efficiency could be found by tuning the stopping condition for the fixed point iteration, but we defer consideration of efficiency to future work.

The resulting coefficient matrix is tridiagonal for the one-dimensional case; however, the coefficient matrix changes at each time step as the pressure, density, permeability, viscosity, porosity, and compressibility data are changed at each time step with the change in pressure. The right-hand side vector also changes. Standard approaches (such as multigrid) can be used to solve the resulting linear systems efficiently at each time step and for each linearization once the matrix and right-hand side have been computed; here, we use direct solvers due to their optimal scaling for one-dimensional problems. As time passes, the cost to compute the right-hand side vector increases because of the dependence of the fractional derivative of the pressure gradient at each spatial point on the values of the pressure gradient at this point at all earlier times. To address this cost, Gaspar et al. [38] developed a parallel-in-time multigrid algorithm based on the waveform relaxation approach to solve time-fractional problems. For uniform space-time grids, the method has a computational cost of $O(N_x N_t \log(N_t))$ operations. The extension of this approach to the graded mesh case would greatly improve the efficiency of these calculations.

## 2.5 Analytical solution for linear case

In the notation of Eq. 3, we consider the simple linear equation that arises with $C_1 = C_2 = 1$ and the domain $0 < x < 1$, $0 < t < 1$. The initial condition is taken to be $p(x, 0) = x(1 - x)$ and the boundary conditions are taken as $p(0, t) = p(1, t) = 0$. The Riemann-Liouville definition for the fractional-order derivative is utilized. The analytical solution is found to be (details shown in Appendix A, Eq. A3):

$$p(x,t) = \sum_{k=1}^{\infty} \frac{4}{k^3\pi^3}\left[1-(-1)^k\right] \times E_{1-\alpha}\left(-k^2\pi^2 t^{1-\alpha}\right)\sin(k\pi x),$$

where $E_{1-\alpha}(s)$ is the Mittag-Leffler function and is defined for $(1-\alpha) > 0$ as

$$E_{1-\alpha}(s) = \sum_{k=0}^{\infty} \frac{s^k}{\Gamma\left((1-\alpha)k+1\right)}.$$

### 2.6 Comparison of errors found from uniform and graded meshes

Figures 2 and 3 compare the errors found using uniform and graded meshes for different values of fractional order, $\alpha$, and for different number of grid points in space for the linear model problem presented above. It is found that in both cases, the graded mesh gives smaller errors than the uniform mesh, except when $\alpha = 0$, where the graded mesh coincides with the uniform mesh. We note that, in Figs. 2 and 3, the shape of the error line found for $\alpha = 0.75$ and a graded mesh is different from the other error lines, depicting that the error reaches a minimum value at $N_t = 6400$, and then starts to increase. We observe that roundoff error starts to dominate in this case, with very small time steps seen on the graded meshes (see Fig. 4). We leave the practical question of how to reliably compute with "large" values of $\alpha$ to future work.

We compute orders of discretization accuracy from the relationship between error and number of time steps for different numbers of grid points in space. Here, we plot the error versus number of time steps on a log-log graph, and the slope of the best fit line gives the order of accuracy. Table 1 compares the order of accuracies of the numerical models developed using uniform and graded meshes, showing that the numerical model developed using uniform meshes is $(1-\alpha)$th-order accurate in time, and that developed using graded meshes is first-order accurate in time.

### 2.7 Verification of the model for the nonlinear case

Equation 3 becomes nonlinear when $C_1$ and/or $C_2$ depend on the pressure. For the nonlinear case, the model is verified using a manufactured solution and comparing that solution with the numerical solution of the modified equation. As a simple nonlinear model, we consider $\rho$ to be a simple function of $p$, while other parameters are kept constant. For the nonlinear formulation, a manufactured solution is obtained by adding a forcing function to Eq. 1.

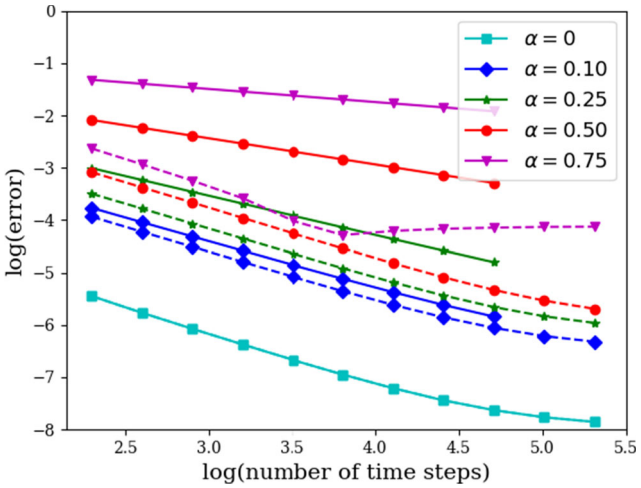


**Fig. 2** Comparison of the maximum norm error values for uniform and graded meshes ($N_x = 100$). Solid lines correspond to uniform meshes and dashed lines to graded meshes

Taking $\rho = 1 - 0.137p$ (see Appendix B), unit values for $\phi$, $c_t$, $\mu$, and $k$, Eq. 1 becomes

$$\frac{\partial}{\partial x}\left[\rho\frac{\partial^\alpha}{\partial t^\alpha}\left(\frac{\partial p}{\partial x}\right)\right] = \rho\frac{\partial p}{\partial t}. \tag{16}$$

The initial condition and boundary conditions are taken to be $p(x,0) = \sin(\pi x)$ and $p(0,t) = p(1,t) = 0$, respectively. The solution is then taken to be $p(x,t) = E_{1-\alpha}\left(-\pi^2 t^{1-\alpha}\right)\sin(\pi x)$, and Eq. 16 is modified via the method of manufactured solutions to be

$$\frac{\partial}{\partial x}\left[\rho\frac{\partial p}{\partial x}\right] = \rho\frac{\partial p}{\partial t} + \pi^2 e^{-\pi^2 t}\left[-\sin(\pi x) - 0.137e^{-\pi^2 t}\cos(2\pi x)\right] + \pi^2\sin(\pi x)e^{-\pi^2 t} \times\left[1 - 0.137e^{-\pi^2 t}\sin(\pi x)\right],$$

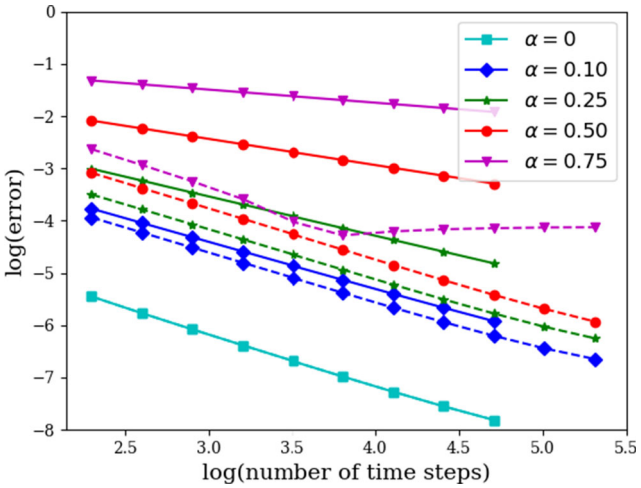


**Fig. 3** Comparison of the maximum norm error values for uniform and graded meshes ($N_x = 200$). Solid lines correspond to uniform meshes and dashed lines to graded meshes

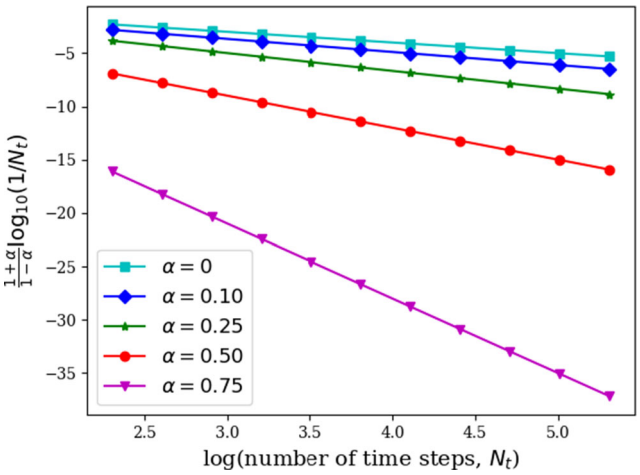


**Fig. 4** Minimum time step size for graded meshes

in the case of $\alpha = 0$ and

$$\frac{\partial}{\partial x}\left[\rho\frac{\partial^\alpha}{\partial t^\alpha}\left(\frac{\partial p}{\partial x}\right)\right] = \rho\frac{\partial p}{\partial t} - 0.137\pi^2 t^{-\alpha} E_{1-\alpha}\left(-\pi^2 t^{1-\alpha}\right) \times E_{1-\alpha,1-\alpha}\left(-\pi^2 t^{1-\alpha}\right)\cos^2(\pi x)$$

for $0 < \alpha < 1$. Again, we consider the domain $0 < x < 1$, $0 < t < 1$.

Figures 5 and 6 show the variation of error found comparing the numerical solutions of the modified equations with the manufactured solutions for different numbers of time steps, and varying $\alpha$ values for both uniform and graded meshes. Here, the one-dimensional space in Figs. 5 and 6 is divided into 100 and 200 grid-points, respectively. It is found that, as the number of time steps is increased, the error decreases linearly at first. However, for larger numbers of time steps, the rate of change in error decreases and, at some point, the error values reach a plateau when the spatial discretization error starts to dominate. The change in error with the number of time steps implies that the numerical model is consistent. The figures show that the numerical model gives the least error for $\alpha = 0$. With increases in $\alpha$, the model gives larger errors, as in the linear case. Like the linear case, we find a different shape of the error line for $\alpha = 0.75$ and a graded mesh, showing that the error reaches a minimum value at $N_t = 6400$, and then starts to increase due to dominant roundoff error. Use of graded meshes makes the errors smaller for all values of $\alpha$, except $\alpha = 0$, where the graded mesh and uniform mesh coincide.

We tabulate the order of temporal accuracies of the numerical model developed using uniform and graded meshes for the nonlinear case for different $\alpha$ values in Table 2. This table shows that the numerical model developed using uniform meshes is $(1-\alpha)$th-order accurate in time, and that developed using graded meshes is first-order accurate in time in the nonlinear case, as in the linear case. However, we note that the graded meshes used here depend on the known behavior of the manufactured solutions and do not give first-order temporal accuracy when the mesh is not graded to fit the decay rate of the solution. It is critical that the grading in the mesh be compatible with the temporal behavior of the solution. Here, for validation, we have used manufactured solutions that mimic the linear case, but further analysis is needed for the general non-linear case.

## 3 Determination of the value of $\alpha$ from experimental data

Iaffaldano et al. [8] designed an experiment to measure volumetric flux through a porous layer while keeping the pressure difference constant between the boundary surfaces. Figure 7 shows the experimental device used in their study. Water-saturated sand is used in the cell for the medium. A cylinder-shaped metal box of height 11.6 cm with an inner diameter of 10.1 cm was used to keep the sand in. Dry sand and water were slowly and alternately filled in the empty cell to obtain the condition of saturation. The initial pressure value for water inside the cell is attained by keeping water-taps $R$ and $R_I$ switched on and $R_U$ switched off, until the height of the water

**Table 1** Comparison of order of temporal accuracies for uniform and graded meshes (linear case)

| Value of fractional order, $\alpha$ | Order of temporal accuracy | | | | | |
|---|---|---|---|---|---|---|
| | $N_x = 50$ | | $N_x = 100$ | | $N_x = 200$ | |
| | Uniform | Graded | Uniform | Graded | Uniform | Graded |
| 0 | 1.0195 | 1.0195 | 1.0256 | 1.0256 | 1.0337 | 1.0337 |
| 0.10 | 0.8890 | 0.9273 | 0.9044 | 0.9524 | 0.9083 | 0.9589 |
| 0.25 | 0.7497 | 0.9274 | 0.7536 | 0.9465 | 0.7546 | 0.9515 |
| 0.50 | 0.5006 | 0.9555 | 0.5009 | 0.9683 | 0.5010 | 0.9716 |
| 0.75 | 0.2501 | 1.0464 | 0.2502 | 1.0535 | 0.2502 | 1.0552 |

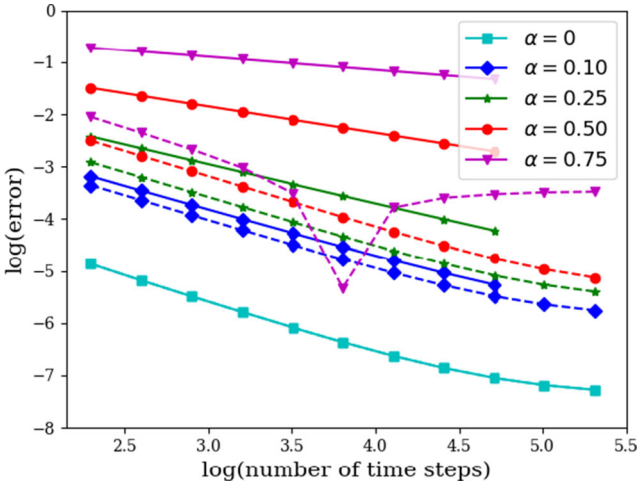


**Fig. 5** maximum norm error values incorporating $\rho = 1 - 0.137p$, and $N_x = 100$. Solid lines correspond to uniform meshes and dashed lines to graded meshes

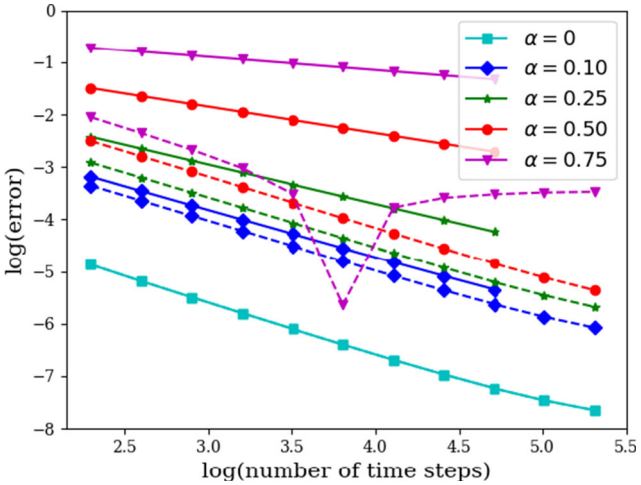


**Fig. 6** maximum norm error values incorporating $\rho = 1 - 0.137p$, and $N_x = 200$. Solid lines correspond to uniform meshes and dashed lines to graded meshes

column, $H$, is obtained. After attaining the same pressure as the initial pressure through the medium, water-tap $R_U$ is opened. This results in atmospheric pressure on the right boundary plane. Since the pressure on the left boundary plane is atmospheric pressure plus the pressure due to the water column of height $H$, the pressure difference is the pressure due to the water column of height $H$, and water starts to flow through the porous medium and runs out from $R_U$. The height of the water column is always $H$ because the surplus water from the water-tap $R$ flows out from the output gate, $U$. Water flow at the right boundary surface was measured by storing water in a small container of known volume, and measuring the relative time interval.

Five different samples of sand were used as the porous layer. The authors presented their experimental results by plotting volumetric flux as a function of elapsed time. The plots presented in [8] are redrawn here in Fig. 8. These experimental results support the idea that permeability may decrease due to the rearrangement of grains and consequent compaction, which was qualitatively shown by Elias and Hajash [39].

Iaffaldano et al. [8] used the empirical Fair and Hatch law (1993) to calculate the permeability, $k$ [40], and found $k = 26$ darcy. They used water of 19 °C as the fluid in all of their experiments. The density and viscosity of water at 19 °C are 0.998408 g/cm$^3$ and 1.0266 cP, respectively. A pressure difference was maintained by exerting an additional pressure equivalent to 212 cm height of the water column (0.20485 atm) at one end. The mass of dry sand used in each experiment was around 1550 g. The density of sand used was 2.4 g/cm$^3$. From this information, the porosity in the sand medium within the cylinder-shaped metal box can be calculated as 30.51%.

The diffusivity equation (Eq. 1) from [10] is based on the following equation that relates volumetric flux to the pressure gradient,

$$u = -\frac{k}{\mu}\tau^{\alpha}\left[\frac{\partial^{\alpha}}{\partial t^{\alpha}}\left(\frac{\partial p}{\partial x}\right)\right]. \tag{17}$$

Using the Riemann-Liouville definition of the fractional-order derivative, Eq. 17 can be written as

$$\begin{aligned} u = -\frac{k}{\mu}\tau^{\alpha}\frac{1}{\Gamma(2-\alpha)}\Bigg[&\frac{(1-\alpha)\frac{\partial p}{\partial x}(t=0)}{(t_n)^{\alpha}} \\ &+\sum_{j=0}^{n-1}\frac{\frac{\partial p}{\partial x}(t=t_{j+1})-\frac{\partial p}{\partial x}(t=t_j)}{t_{j+1}-t_j} \\ &\times\left((t_n-t_j)^{1-\alpha}-(t_n-t_{j+1})^{1-\alpha}\right)\Bigg]. \end{aligned} \tag{18}$$

Since the pressure gradient is kept constant in the experiment, Eq. 18 can be written as

$$u = -\frac{k}{\mu}\frac{(1-\alpha)}{\Gamma(2-\alpha)}\frac{\tau^{\alpha}}{(t_n)^{\alpha}}\frac{\partial p}{\partial x}(t=0). \tag{19}$$

Substitution of the permeability, viscosity, and pressure gradient with their numerical values in Eq. 19 gives

$$u = (0.44726)\frac{(1-\alpha)}{\Gamma(2-\alpha)}\frac{\tau^{\alpha}}{(t_n)^{\alpha}}. \tag{20}$$

Equation 20 can be written as

$$\log(u) = \log\left(0.44726\frac{(1-\alpha)}{\Gamma(2-\alpha)}\tau^{\alpha}\right) - \alpha\log(t_n). \tag{21}$$

We calculate the values of $\alpha$ and $\tau$ with least-squares regression analysis using the data obtained from the

**Table 2** Comparison of order of temporal accuracies for uniform and graded meshes (nonlinear case)

| Value of fractional order, $\alpha$ | Order of temporal accuracy | | | | | |
|---|---|---|---|---|---|---|
| | $N_x = 50$ | | $N_x = 100$ | | $N_x = 200$ | |
| | Uniform | Graded | Uniform | Graded | Uniform | Graded |
| 0 | 0.9947 | 0.9947 | 1.0253 | 1.0253 | 1.0334 | 1.0334 |
| 0.10 | 0.8920 | 0.9302 | 0.9066 | 0.9540 | 0.9103 | 0.9602 |
| 0.25 | 0.7535 | 0.9300 | 0.7572 | 0.9481 | 0.7581 | 0.9528 |
| 0.50 | 0.5069 | 0.9583 | 0.5073 | 0.9703 | 0.5073 | 0.9734 |
| 0.75 | 0.2526 | 1.0690 | 0.2527 | 1.0760 | 0.2527 | 1.0777 |

experiments. Calculation for $\alpha$ and $\tau$ gives the values tabulated in Table 3. The larger relaxation time for the first experiment reflects the requirement of a longer time for this experiment to return into equilibrium from a perturbed condition compared to the other experiments. The average value of $\alpha$ is found to be around 0.05. Iaffaldano et al. [8] calculated the value of fractional order in their model to be 0.53; however, the Caputo fractional derivative was used in the formulation from [8], whereas we consider the Riemann-Liouville fractional derivative and [8] used a slightly different model. Hence, the value of fractional order calculated in [8] is different from that calculated here.

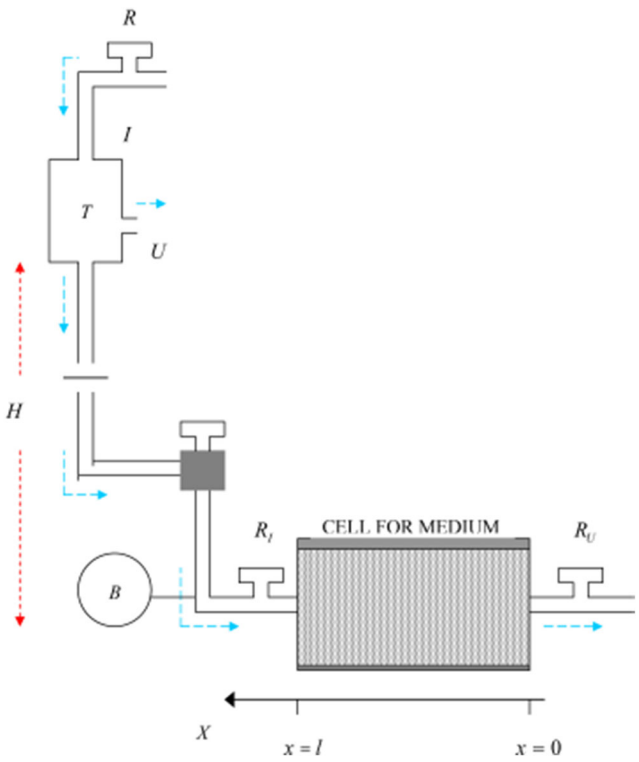


**Fig. 7** Experimental device used in experiment of Iaffaldano et al. (from [8])

## 4 Simulation of experimental data

### 4.1 Optimal number of time steps for graded meshes

Considering the value of the fractional order, $\alpha \approx 0.05$, found in the previous section, Table 4 shows the order of spatial accuracy for graded meshes for this value of $\alpha$ and the initial condition $p(x, 0) = x(1 - x)$. It is found that the order of spatial accuracy of the discretization method approaches two when large numbers of time steps are used. In addition, the discretization method used in the numerical model is first-order accurate in time. Hence, the optimal relationship between the number of grid points in space and number of steps in time should be taken to be $N_t = \beta N_x^2$. The best value of $\beta$, the proportionality constant between $N_t$ and $N_x^2$, can be found looking at the computed error values.

Figure 2 shows that, for $N_x = 100$, the rate of change in error slows beyond $N_t = 51200$ indicating spatial discretization error becomes dominant here. The optimal number of time steps in this case can be taken in the range of $25600 - 51200$. Hence, the optimal value of $\beta$ for $N_x = 100$ lies in the range of 2 to 5. Similarly, from Fig. 3, the optimal range of number of time steps in unit time for $N_x = 200$ is $25600 - 102400$. Therefore, the ideal value of $\beta$ for $N_x = 200$ is in the range of 1 to 3. In what follows, we fix $\beta = 2$ to approximate the value of $N_t$ from $N_x$ while using our numerical model to calculate pressure values in each grid cell in each time step.

### 4.2 Simulated and experimental flux values

Figure 8 shows the simulated flux values for both the overall average value of $\alpha = 0.05$, and the values of $\alpha$ given for each experiment in Table 3 and computed $\tau$ values. The pressure values in each grid cell in each time step, required to calculate flux values, are computed using the numerical model that was developed using graded meshes. The length of (each) grid cell was taken to be 0.02 cm giving $N_x = 580$. The length of $n$th time step is calculated as,

**Table 3** Computed values of $\alpha$ and $\tau$

| Experiment No. | Fractional order, $\alpha$ | Relaxation time, $\tau$ (s) |
|---|---|---|
| 1 | 0.050348217 | 2076.38 |
| 2 | 0.023771495 | 132.80 |
| 3 | 0.038373096 | 244.44 |
| 4 | 0.034639443 | 160.06 |
| 5 | 0.075865421 | 802.63 |

$\Delta t_n = t_n - t_{n-1}$, where $t_n = T(n/N_t)^{\omega}$, $n = 0, 1, 2, ..., N_t$, and $\omega = (1 + \alpha)/(1 - \alpha)$. The values of $T$ are taken as 39670, 32460, 39000, 39630, and 38930 s for the first through fifth experiment, respectively. Figure 8 compares the simulated flux values with those obtained from the experiments. It is found that the simulated values are very close to experimental values. The figure also presents the flux calculated from Darcy's law without the fractional derivative terms, showing the improved physical accuracy gained by including the memory term. Perhaps counter-intuitively, we see that the simulation results with $\alpha = 0.05$ generally outperform those with the value of $\alpha$ obtained by regression from the data for each experiment. Since all five experiments used samples of sand with similar properties, it is reasonable to expect the variations in $\alpha$ obtained for each experiment to be statistical in nature, and an averaged value to provide a better overall fit to the data.

## 5 Conclusions

Numerical models have been developed to solve a time-fractional nonlinear diffusion equation applying the Riemann-Liouville definition for the fractional-order derivative using uniform and graded meshes. It is found that the numerical model developed using graded meshes gives smaller errors compared to that using uniform meshes, extending the theoretical work of [34] to the practical setting of flow through porous media. The value of fractional order used in the mathematical model has been computed to be about 0.05 using experimental data collected from literature. The study recommends utilizing graded meshes instead of uniform meshes for better accuracy, although we note the improvement offered for small $\alpha$ is not overwhelming. This research initiates the first step towards the development of a large-scale memory-based reservoir simulator solving the memory-based diffusion equation and computing the value of fractional order in the equation. Further work is required to make the computational algorithm efficient. In addition, significant research work is required to develop a complete memory-based reservoir simulator.

## Appendix A

To find an analytical solution, we consider $C_1 = C_2 = 1$ in Eq. 3 giving

$$\frac{\partial}{\partial x}\left[\frac{\partial^{\alpha}}{\partial t^{\alpha}}\left(\frac{\partial p}{\partial x}\right)\right] = \frac{\partial p}{\partial t}, \tag{A1}$$

with boundary conditions $p(0) = p(1) = 0$. We write the solution in series form as

$$p(x,t) = \sum_{k=1}^{\infty} T_k(t)\sin(k\pi x),$$

noting that

$$\frac{\partial p}{\partial t}(x,t) = \sum_{k=1}^{\infty} T_k'(t)\sin(k\pi x) = -\sum_{k=1}^{\infty} k^2\pi^2 \frac{\partial^{\alpha} T_k(t)}{\partial t^{\alpha}}\sin(k\pi x) = \frac{\partial}{\partial x}\left[\frac{\partial^{\alpha}}{\partial t^{\alpha}}\left(\frac{\partial p}{\partial x}\right)\right].$$

To be a solution, we require that

$$T_k'(t) = -k^2\pi^2 \frac{\partial^{\alpha} T_k(t)}{\partial t^{\alpha}},$$

**Table 4** Order of spatial accuracy for graded meshes comparing $N_x = 100$ and $N_x = 200$

| $N_t$ | Order of spatial accuracy | | | |
|---|---|---|---|---|
| | $\alpha = 0$ | $\alpha = 0.10$ | $\alpha = 0.25$ | $\alpha = 0.50$ |
| 12800 | 1.8581 | 1.7712 | 1.7071 | 1.5971 |
| 25600 | 1.9441 | 1.8770 | 1.8389 | 1.7722 |

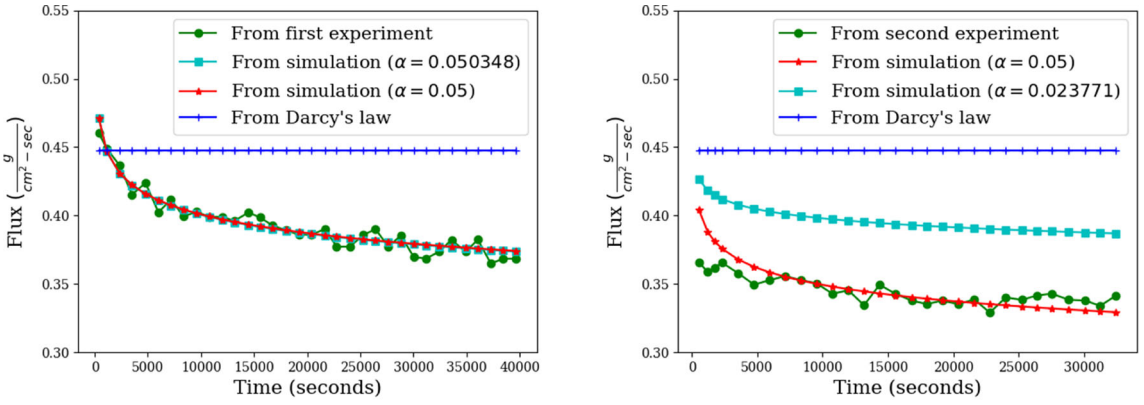


(a) For first experiment




(b) For second experiment

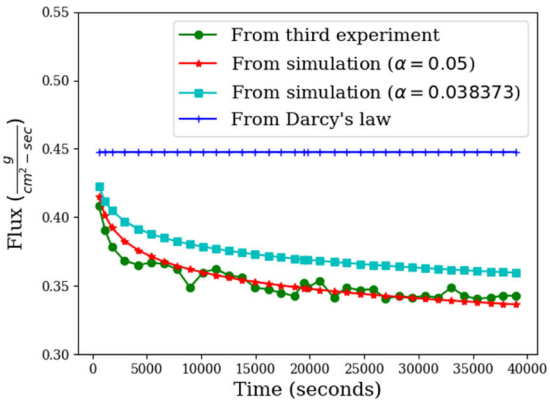


(c) For third experiment

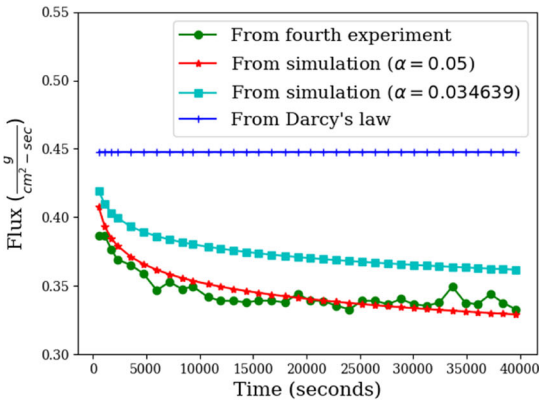


(d) For fourth experiment

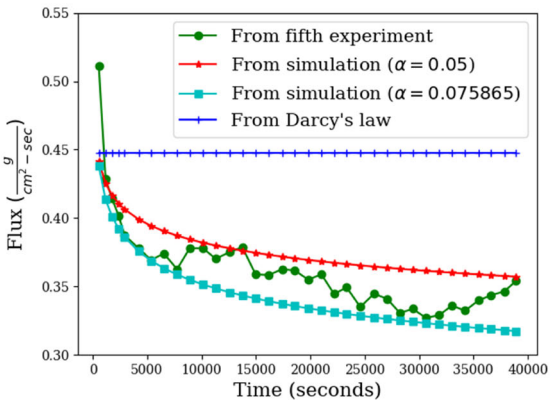


(e) For fifth experiment

**Fig. 8** Flux values from the experiments, simulation, and Darcy's law

and that

$$T_k(0) = \beta_k,$$

where $\beta_k$ comes from the sine series expansion of the initial data, $p(x,0) = \sum_{k=1}^{\infty} \beta_k \sin(k\pi x)$. Taking Laplace transforms, we have

$$\mathscr{L}\left[T_k'(t)\right] = s\widehat{T}_k(s) - \beta_k.$$

For the Riemann-Liouville definition of the fractional-order derivative,

$$\mathscr{L}\left[\frac{\partial^\alpha T_k(t)}{\partial t^\alpha}\right] = s^\alpha \widehat{T}_k(s) - \left[D^{\alpha-1}T_k(t)\right]_{t=0}. \tag{A2}$$

Therefore,

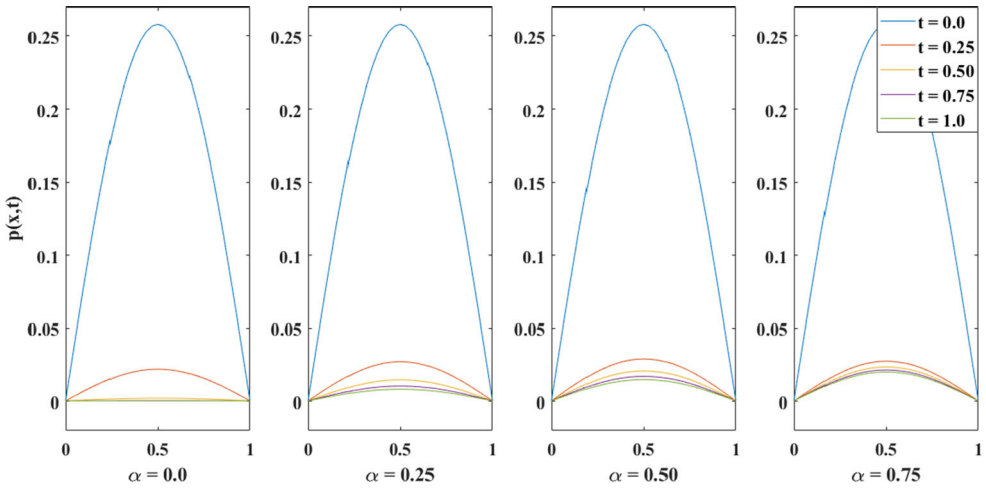


**Fig. 9** Analytical solution (Eq. A3) of Eq. A1 for different values of $\alpha$

$$s\widehat{T}_k(s) - \beta_k = -k^2\pi^2\left(s^\alpha \widehat{T}_k(s) - c_k\right)$$

$$\text{where} \quad c_k = \left[D^{\alpha-1}T_k(t)\right]_{t=0}$$

$$\text{or,} \quad \widehat{T}_k(s) = \frac{\beta_k + k^2\pi^2 c_k}{s + k^2\pi^2 s^\alpha} = \frac{(\beta_k + k^2\pi^2 c_k)s^{-\alpha}}{s^{1-\alpha} + k^2\pi^2}.$$

This gives

$$T_k(t) = \left(\beta_k + k^2\pi^2 c_k\right) E_{1-\alpha}\left(-k^2\pi^2 t^{1-\alpha}\right),$$

where $E_{1-\alpha}(v)$ is the Mittag-Leffler function, and is defined for $(1-\alpha)>0$ as

$$E_{1-\alpha}(v) = \sum_{k=0}^{\infty} \frac{v^k}{\Gamma\left((1-\alpha)\,k+1\right)},$$

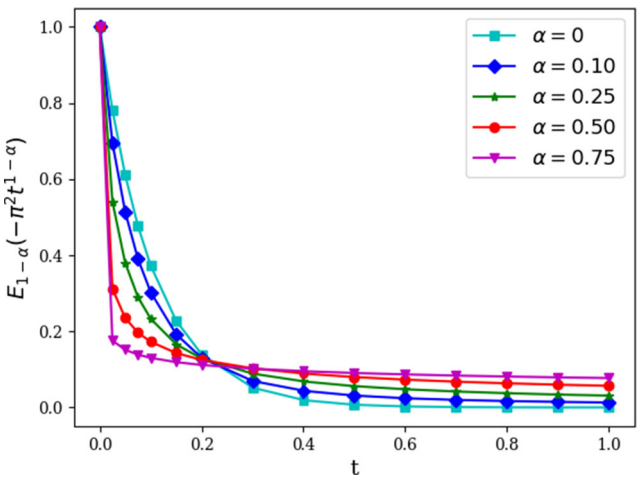


**Fig. 10** Change in the values of $E_{1-\alpha}(-\pi^2 t^{1-\alpha})$ with $t$ for different $\alpha$ values. For $\alpha = 0$, $E_{1-\alpha}(-\pi^2 t^{1-\alpha}) = e^{-\pi^2 t}$

since $\quad \mathscr{L}\left[E_{1-\alpha}\left(-k^2\pi^2 t^{1-\alpha}\right)\right] = \frac{s^{-\alpha}}{s^{1-\alpha} + k^2\pi^2}.$

Now,

$$D^{\alpha-1}\left[(\beta_k + k^2\pi^2 c_k)E_{1-\alpha}(-k^2\pi^2 t^{1-\alpha})\right] = \frac{\beta_k + k^2\pi^2 c_k}{-k^2\pi^2}\left(E_{1-\alpha}\left(-k^2\pi^2 t^{1-\alpha}\right) - 1\right),$$

which forces $D^{\alpha-1}\left[T_k(t)\right]_{t=0} = 0$ as $E_{1-\alpha}(0) = 1$, giving $c_k = 0$, $T_k(t) = \beta_k E_{1-\alpha}\left(-k^2\pi^2 t^{1-\alpha}\right)$, and

$$p(x,t) = \sum_{k=1}^{\infty} \beta_k E_{1-\alpha}\left(-k^2\pi^2 t^{1-\alpha}\right)\sin(k\pi x). \tag{A3}$$

Equation A3 is the general analytical solution of Eq. A1 for any initial condition. Now, taking the initial condition considered above,

$$p_0(x) = x(1-x),$$

we have (from standard orthogonality)

$$\beta_k = \frac{\int_0^1 p_0(x)\sin(k\pi x)\,dx}{\int_0^1 \sin^2(k\pi x)\,dx}.$$

Calculation gives

$$\beta_k = \frac{4}{k^3\pi^3}\left[1 - (-1)^k\right]. \tag{A4}$$

Note also that were we to replace the Riemann-Liouville definition of the fractional order derivative by the Caputo definition, Eq. A2 would be replaced by

$$\mathscr{L}\left[\frac{\partial^\alpha T_k(t)}{\partial t^\alpha}\right] = s^\alpha \widehat{T}_k(s) - s^{\alpha-1}\beta_k,$$

leading to

$$p(x,t) = p(x,0),$$

which is a constant-in-time solution. Here, we see that this constant-in-time solution must arise when the Caputo derivative is used in the fractional diffusion equation containing a first derivative in time and the fractional derivative mixed within the spatial derivatives.

Cross-sections of the analytical solution given in Eq. A3 for $\beta_k$ as in Eq. A4 are plotted in Fig. 9 for different values of $\alpha$. These plots show that the inclusion of a temporal derivative of order $\alpha$ result in solutions that dampen more quickly towards constant solutions, and that higher values of $\alpha$ lead to faster initial decay. This is emphasized in Fig. 10, where we plot the temporal behavior of the dominant term in Eq. A3, showing the fast initial decay for $\alpha > 0$. This behavior of the fractional temporal derivative makes the solution difficult to approximate on uniform meshes. Hence, it is helpful to grade the temporal mesh so that the time steps are smaller in the beginning.

## Appendix B

We compute density values at different pressures below bubblepoint pressure using the correlations developed in [41]. From the given density and pressure values, we find the linear equation of best fit as

$$\rho = 0.7298 - 0.0004p, \tag{B1}$$

where $\rho$ is in $g/cc$, and $p$ is in atm. This relation is derived by considering "typical" values for the physical variables, of reservoir temperature $= 185\ ^0F$, stock tank oil gravity $= 43.7\ ^0API$, solution gas-oil ratio at bubble point pressure $= 941\ scf/stb$, gas specific gravity measured at separator $= 0.735$, and gas specific gravity $= 0.865$. Rescaling $x$, $t$, $p$, $\rho$ as $\hat{x} = \frac{x}{x_{max}}$, $\hat{t} = \frac{t}{t_{max}}$, $\hat{p} = \frac{p}{p_i}$, $\hat{\rho} = \frac{\rho}{0.7298}$, respectively and taking $p_i = 250\ atm$ $(3650\ psi)$, Eq. B1 can be written as

$$\hat{\rho} = 1 - 0.137\hat{p}. \tag{B2}$$

We use Eq. B2 on a nondimensional unit domain in Section 2.7.

**Acknowledgments** The authors would like to thank the Natural Sciences and Engineering Research Council of Canada (NSERC); Research and Development Corporation of Newfoundland and Labrador (RDC), funding no. 210992; and Statoil Canada Ltd., funding no. 211162 for providing financial support to accomplish this research. The work of Scott MacLachlan was partially supported by an NSERC Discovery Grant.

## References

1. Caputo, M.: Diffusion of fluids in porous media with memory. Geothermics **28**(1), 113–130 (1999)
2. Caputo, M.: Models of flux in porous media with memory. Water Resour. Res. **36**(3), 693–705 (2000)
3. Christensen, R.: Theory of viscoelasticity: an introduction. Elsevier, Amsterdam (2012)
4. Hossain, M.E., Mousavizadegan, S.H., Ketata, C., Islam, M.R.: A novel memory based stress strain model for reservoir characterization. Nat Sci Sustainable Technol Res Prog **1**, 1–29 (2008)
5. Zavala-Sanchez, V., Dentz, M., Sanchez-Vila, X.: Characterization of mixing and spreading in a bounded stratified medium. Adv. Water Resour. **32**(5), 635–648 (2009)
6. Zhang, H.M.: Driver memory, traffic viscosity and a viscous vehicular traffic flow model. Transp. Res. B Methodol. **37**(1), 27–41 (2003)
7. Caputo, M., Plastino, W.: Diffusion in porous layers with memory. Geophys. J. Int. **158**(1), 385–396 (2004)
8. Iaffaldano, G., Caputo, M., Martino, S.: Experimental and theoretical memory diffusion of water in sand. Hydrol. Earth Syst. Sci. Discuss. **2**(4), 1329–1357 (2005)
9. Di Giuseppe, E., Moroni, M., Caputo, M.: Flux in porous media with memory: models and experiments. Transp. Porous Media **83**(3), 479–500 (2010)
10. Hossain, M.E., Mousavizadegan, S.H., Islam, M.R., et al.: A new porous media diffusivity equation with the inclusion of rock and fluid memories. E-Library, SPE– 114287 (2008)
11. Abu-Saman, A.M., Assaf, A.M.: Stability and convergence of Crank-Nicholson method for fractional advection dispersion equation. Advances in Applied Mathematical Analysis **2**(2), 117–125 (2007)
12. Chen, C.-M., Liu, F., Turner, I., Anh, V.: A Fourier method for the fractional diffusion equation describing sub-diffusion. J. Comput. Phys. **227**(2), 886–897 (2007)
13. Chen, S., Liu, F., Zhuang, P., Anh, V.: Finite difference approximations for the fractional Fokker–Planck equation. Appl. Math. Model. **33**(1), 256–273 (2009)
14. Chen, C.-M., Liu, F., Anh, V., Turner, I.: Numerical schemes with high spatial accuracy for a variable-order anomalous subdiffusion equation. SIAM J. Sci. Comput. **32**(4), 1740–1760 (2010)
15. Cui, M.: Compact finite difference method for the fractional diffusion equation. J. Comput. Phys. **228**(20), 7792–7804 (2009)
16. Du, R., Cao, W.R., Sun, Z.Z.: A compact difference scheme for the fractional diffusion-wave equation. Appl. Math. Model. **34**(10), 2998–3007 (2010)
17. Gao, G.-H., Sun, Z.-Z.: A compact finite difference scheme for the fractional sub-diffusion equations. J. Comput. Phys. **230**(3), 586–595 (2011)
18. Langlands, T.AM., Henry, B.I.: The accuracy and stability of an implicit solution method for the fractional diffusion equation. J. Comput. Phys. **205**(2), 719–736 (2005)
19. Liu, F., Zhuang, P., Anh, V., Turner, I.: A fractional-order implicit difference approximation for the space-time fractional diffusion equation. ANZIAM Journal **47**, 48–68 (2006)
20. Liu, Q., Gu, Y., Zhuang, P., Liu, F., Nie, Y.F.: An implicit RBF meshless approach for time fractional diffusion equations. Comput. Mech. **48**(1), 1–12 (2011)
21. Lynch, V.E., Carreras, B.A., del Castillo-Negrete, D., Ferreira-Mejias, K.M., Hicks, H.R.: Numerical methods for the solution of partial differential equations of fractional order. J. Comput. Phys. **192**(2), 406–421 (2003)
22. Meerschaert, M.M., Tadjeran, C.: Finite difference approximations for fractional advection–dispersion flow equations. J. Comput. Appl. Math. **172**(1), 65–77 (2004)

23. Murillo, J.Q., Yuste, S.B.: On three explicit difference schemes for fractional diffusion and diffusion-wave equations. Phys. Scr. **2009**(T136), 014025 (2009)
24. Murillo, J.Q., Yuste, S.B.: An explicit difference method for solving fractional diffusion and diffusion-wave equations in the Caputo form. J. Comput. Nonlinear Dyn. **6**(2), 021014 (2011)
25. Sun, Z.-Z., Wu, X.: A fully discrete difference scheme for a diffusion-wave system. Appl. Numer. Math. **56**(2), 193–209 (2006)
26. Tadjeran, C., Meerschaert, M.M., Scheffler, H.-P.: A second-order accurate numerical approximation for the fractional diffusion equation. J. Comput. Phys. **213**(1), 205–213 (2006)
27. Wang, K., Wang, H.: A fast characteristic finite difference method for fractional advection–diffusion equations. Adv. Water Resour. **34**(7), 810–816 (2011)
28. Yuste, S.B., Acedo, L.: An explicit finite difference method and a new Von Neumann-type stability analysis for fractional diffusion equations. SIAM J. Numer. Anal. **42**(5), 1862–1874 (2005)
29. Zhuang, P., Liu, F.: Implicit difference approximation for the time fractional diffusion equation. J. Appl. Math. Comput. **22**(3), 87–99 (2006)
30. Zhuang, P., Liu, F., Anh, V., Turner, I.: New solution and analytical techniques of the implicit numerical method for the anomalous subdiffusion equation. SIAM J. Numer. Anal. **46**(2), 1079–1095 (2008)
31. Deng, W.: Finite element method for the space and time fractional Fokker–Planck equation. SIAM J. Numer. Anal. **47**(1), 204–226 (2008)
32. Roop, J.P.: Computational aspects of FEM approximation of fractional advection dispersion equations on bounded domains in $R^2$. J. Comput. Appl. Math. **193**(1), 243–268 (2006)
33. Chen, C.-M., Liu, F., Burrage, K.: Finite difference methods and a Fourier analysis for the fractional reaction–subdiffusion equation. Appl. Math. Comput. **198**(2), 754–769 (2008)
34. Stynes, M., O'Riordan, E., Gracia, J.L.: Error analysis of a finite difference method on graded meshes for a time-fractional diffusion equation. SIAM J. Numer. Anal. **55**(2), 1057–1079 (2017)
35. Oldham, K., Spanier, J.: The fractional calculus theory and applications of differentiation and integration to arbitrary order. Elsevier, Amsterdam, vol. 111 (1974)
36. Sochi, T.: Non-Newtonian flow in porous media. Polymer **51**(22), 5007–5023 (2010)
37. Caputo, M.: Diffusion with space memory modelled with distributed order space fractional differential equations. Annals of Geophysics, 46(2) (2003)
38. Gaspar, F.J., Rodrigo, C.: Multigrid waveform relaxation for the time-fractional heat equation. SIAM J. Sci. Comput. **39**(4), A1201–A1224 (2017)
39. Elias, B.P., Hajash, A.: Changes in quartz solubility and porosity due to effective stress: An experimental investigation of pressure solution. Geology **20**(5), 451–454 (1992)
40. Bear, J.: Dynamics of fluids in porous media. Courier Corporation, North Chelmsford (2013)
41. Velarde, J., Blasingame, T.A., McCain, W.D. Jr., et al: Correlation of black oil properties at pressures below bubble point pressure-a new approach. Annual Technical Meeting, Petroleum Society of Canada (1997)